Supplemental Materials: Topological Phase Transitions Induced by Disorder in Magnetically Doped Topological Insulator (Bi, Sb)$_2$Te$_3$ Thin Films

Takuya Okugawa,[1] Peizhe Tang,[2,3,*] Angel Rubio,[3,4,5] and Dante M. Kennes[1,3,†]

[1] *Institut für Theorie der Statistischen Physik, RWTH Aachen, 52056 Aachen, Germany and JARA - Fundamentals of Future Information Technology.*
[2] *School of Materials Science and Engineering, Beihang University, Beijing 100191, P. R. China.*
[3] *Max Planck Institute for the Structure and Dynamics of Matter, Center for Free Electron Laser Science, 22761 Hamburg, Germany.*
[4] *Center for Computational Quantum Physics, Simons Foundation Flatiron Institute, New York, NY 10010 USA*
[5] *Nano-Bio Spectroscopy Group, Departamento de Fisica de Materiales, Universidad del País Vasco, UPV/EHU- 20018 San Sebastián, Spain*

(Dated: September 30, 2020)

I. REAL SPACE FORMULATION OF THE MODEL

The lattice version of the Hamiltonian of Eq. (1) of the main text is given by

$$H_0 = \begin{pmatrix} h(\boldsymbol{k}) + gM\sigma_z & 0 \\ 0 & h^*(\boldsymbol{k}) - gM\sigma_z \end{pmatrix} \tag{S.1}$$

$$h(\boldsymbol{k}) = \boldsymbol{d}(\boldsymbol{k}) \cdot \boldsymbol{\sigma} \tag{S.2}$$

$$\boldsymbol{d}(\boldsymbol{k}) = [v_F a^{-1} \sin(k_y a), -v_F a^{-1} \sin(k_x a), m(\boldsymbol{k})] \tag{S.3}$$

$$m(\boldsymbol{k}) = m_0 + 2Ba^{-2}[2 - \cos(k_x a) + \cos(k_y a)], \tag{S.4}$$

where a is the lattice constant and we take $a = 2$ nm for all of our calculations. Obviously, Eq. (S.1) reduces to Eq. (1) of the main text if expanded to second order around $k_x = k_y = 0$, i.e. around the Γ-point. In the momentum space, We define the respective dispersions $E^{u/l} = \pm\sqrt{(v_F k)^2 + m^{u/l}(\boldsymbol{k})^2}$, where $m^{u/l}(\boldsymbol{k}) = m(\boldsymbol{k}) \pm gM$.

Furthermore, in order to model disorder effects, we transform Eq. (S.1) to real space obtaining a square lattice with:

$$H_0 = \Sigma_{ii'jj'} H_{ii'jj'} c^\dagger_{i'j'} c_{ij} \tag{S.5}$$

$$\begin{aligned} H_{ii'jj'} = {} & M\delta_{ii'}\delta_{jj'} + P_x\delta_{i+1i'}\delta_{jj'} + P_x^\dagger\delta_{ii'+1}\delta_{jj'} \\ & + P_y\delta_{ii'}\delta_{j+1j'} + P_y^\dagger\delta_{ii'}\delta_{jj'+1} \end{aligned} \tag{S.6}$$

$$M = (m_0 + 4B)\Gamma_1 + gM\Gamma_2 \tag{S.7}$$

$$P_x = -B\Gamma_1 - \frac{v_F}{2\mathrm{i}}\Gamma_4 \tag{S.8}$$

$$P_y = -B\Gamma_1 + \frac{v_F}{2\mathrm{i}}\Gamma_3 \tag{S.9}$$

where i and j are the sites' x and y coordinates, respectively. $\Gamma^{1,2,3,4}$ are defined as follows:

$$\Gamma_1 = \begin{pmatrix} \sigma_z & 0 \\ 0 & \sigma_z \end{pmatrix} \tag{S.10}$$

$$\Gamma_2 = \begin{pmatrix} \sigma_z & 0 \\ 0 & -\sigma_z \end{pmatrix} \tag{S.11}$$

$$\Gamma_3 = \begin{pmatrix} \sigma_x & 0 \\ 0 & \sigma_x \end{pmatrix} \tag{S.12}$$

$$\Gamma_4 = \begin{pmatrix} \sigma_y & 0 \\ 0 & -\sigma_y \end{pmatrix} \tag{S.13}$$

The impurities are modeled as randomly distributed on-site potentials drawn from a uniform distribution between $[-W/2, W/2]$. The term to be added to $H_{ii'jj'}$ is explicitly given as:

$$W_{ii'jj'} = \delta_{ii'}\delta_{jj'}W_{ij} \tag{S.14}$$

$$W_{ij} = \begin{pmatrix} W_{ij,+\uparrow} & 0 & 0 & 0 \\ 0 & W_{ij,-\downarrow} & 0 & 0 \\ 0 & 0 & W_{ij,+\downarrow} & 0 \\ 0 & 0 & 0 & W_{ij,-\uparrow}. \end{pmatrix} \tag{S.15}$$

In our work, since non-magnetic impurity are considered, $W_{ij,+\uparrow} = W_{ij,+\downarrow}$ and $W_{ij,-\uparrow} = W_{ij,-\downarrow}$ are used. Adding the disorder amounts to substituting $M \to M + W_{ij}$ in Eq. (S.5) and we employ this Hamiltonian for the central region described in the main text with the number of lattice sites being $N_x = L_x/a$ and $N_y = L_y/a$. For the left and right leads, the clean Hamiltonian of Eq. (S.5) without any disorder is used.

II. SELF-CONSISTENT BORN APPROXIMATION

First, we calculate the static self-energy $\Sigma^{u/l}$ defined by $(E_F - H_0^{u/l} - \Sigma^{u/l})^{-1} = \langle (E_F - H^{u/l})^{-1} \rangle$, where $\langle \cdots \rangle$ and $H_0^{u/l}(H^{u/l})$ denote the disorder average and the upper/lower Block of (S.1) without(with) disorder potential, respectively. Like the Hamiltonian, the self-energy can be decomposed into blocks $\Sigma^{u/l} = \Sigma_0^{u/l}\sigma_0 + \Sigma_x^{u/l}\sigma_x + \Sigma_y^{u/l}\sigma_y + \Sigma_z^{u/l}\sigma_z$, from which the renormalized mass and chemical potential can be defined as $\overline{m}_0^{u/l} = m_0^{u/l} + \Sigma_z^{u/l}$ and $\overline{\mu}^{u/l} = E_F - \Sigma_0^{u/l}$, where $m_0^{u/l} = m_0 \pm gM$ for the upper/lower block. For systems with a finite exchange field the time reversal symmetry is broken and

the renormalization is different for the upper/lower block $\Sigma^u \neq \Sigma^l$. The self-consistent Born approximation, yields

$$\Sigma^{u/l} = \frac{W^2 a^2}{48\pi^2} \lim_{\eta\to 0^+} \int_{\mathrm{FBZ}} d\boldsymbol{k} [E_F + i\eta - H_0^{u/l} - \Sigma^{u/l}]^{-1}, \tag{S.16}$$

with FBZ denoting the first Brillouin zone. Within the Born approximation, a sign change of the effective mass term $\overline{m}_0^{u/l}$ signals a topological phase transition (TPT) induced by the disorder, however, to observe the topologically protected quantized conductance, the effective chemical potential renormalized by disorder must additionally be located in the bulk gap, such that the current is carried exclusively by the edge states. Consequently the phase boundary, reflecting the conductive behavior of the system, is defined by the additional condition $|\overline{\mu}^{u/l}| = -\overline{m}_0^{u/l}$ for $\overline{m}_0^{u/l} < 0$ and $|\overline{\mu}^{u/l}| = \overline{m}_0^{u/l}$ for $\overline{m}_0^{u/l} > 0$.

III. NON-SELF-CONSISTENT SOLUTION OF THE BORN SELF-ENERGY

Neglecting the feedback of $\Sigma^{u/l}$ on the right hand side of Eq. (S.16) and keeping only the logarithmically divergent part of the integral,[1] we can obtain a closed form expression of the renormalized mass term $\overline{m}_0^{u/l}$ and chemical potential $\overline{\mu}^{u/l}$:

$$\overline{m}_0^{u/l} = m_0^{u/l} - \frac{W^2 a^2}{48\pi} \frac{1}{B} \ln \left| \frac{B^2}{E_F^2 - (m_0^{u/l})^2} \left(\frac{\pi}{a}\right)^4 \right| \tag{S.17}$$

$$\bar{\mu} = E_F. \tag{S.18}$$

Eq. (S.17) shows that the disorder effects only the mass and not the chemical potential within the non-self-consistent approach. The change in mass $\delta m_0^{u/l} = \overline{m}_0^{u/l} - m_0^{u/l}$ is found to always be negative for the parameters used in our calculations. This explains the tendency of disorder to promote topologically non-trivial bands in our study of magnetically doped topological insulator (Bi, Sb)$_2$Te$_3$ thin films.

IV. PHASE DIAGRAM OF 4QLS AS A FUNCTION OF DISORDER STRENGTH AND FERMI ENERGY

In Fig. 1 we analyze the 4QLs case. Without exchange field $gM = 0$, shown in panels (a) and (b) we find a QSH insulator (the non-disordered case corresponds to the point D of (f) in Fig. 2 of the main text) with quantized conductance $2e^2/h$ and vanishing standard deviation in the bulk gap window ($|E_F| < 29$ meV). In contrast to the 3QLs case, disorder does not induce any

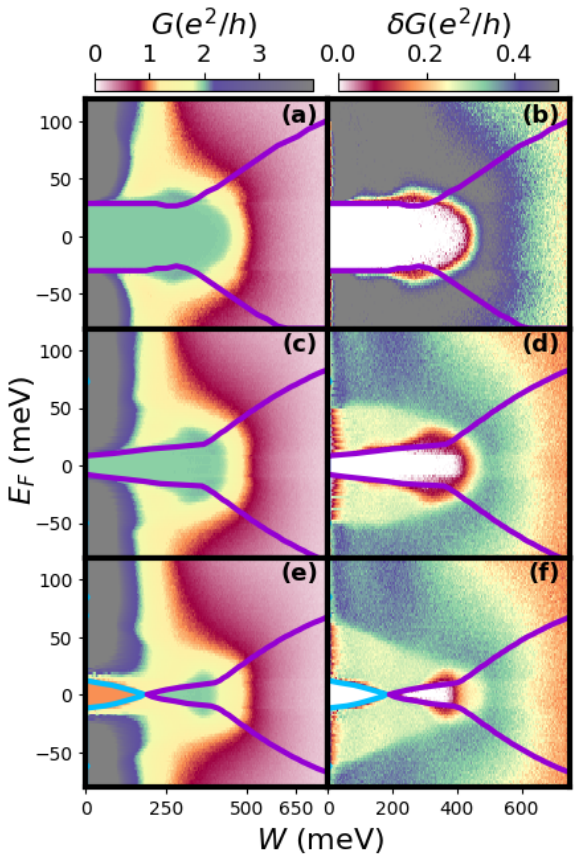

FIG. 1. Left (a), (c), (e) and right (b), (d), (f) panels show the average conductance G and the corresponding standard deviation δG as a function of disorder strength W and Fermi energy E_F for 4QLs (Bi, Sb)$_2$Te$_3$ thin film with and without magnetic doping. The exchange field gM is taken to be (a), (b): 0 meV, (c), (d): 20 meV, and (e), (f): 40 meV. The color lines stand for phase boundaries from self-consistent Born approximation. Details of the colored lines and calculation parameters are shown in Ref. 2. In all calculations, the system sizes are set to $L_x = 400a$ and $L_y = 100a$ and averages over 500 random configuration are performed.

TPTs. This can be understood by the disorder amounting to a negative contribution to the topological mass term within the Born approximation (which is originally negative for 4QLs case). This can be found by using the solution of the closed form of Born approximations after neglecting the self-consistency. The phase boundary between the QSH and the metallic region is well-described by the self-consistent Born approximation while the one between QSH and the Anderson insulator again cannot be obtained by this approximation. Even though panels (c) and (d) show a result similar at face value, it demonstrates the existence of a spin-Chern insulator at finite exchange field gM. This topological state is not altered by weak disorder and slightly widens in the phase diagram up to around $W \approx 300$ meV as disorder is increased. As we discussed in (a), (b), the disorder does not

change the already negative topological mass term to be positive, meaning that once a band inversion occurred, its band does not return to be topologically trivial. The boundary of the spin-Chern insulator and the metal can be explained with the self-consistent Born approximation once more, and when the disorder is increased further, as above, an Anderson insulator is found. Finally, in the panels (e) and (f) the non-disordered state corresponds to a QAH insulator around $E_F = 0$ and we find a similar behavior as in the 3QLs case (compare panels (e) and (f) of Fig. 3 of the main text). The only difference here is the mechanism of how the disorder induces a spin-Chern insulator. Here, at zero disorder the inverted bands from the upper block Hamiltonian was first made trivial by the effects of the exchange field, and upon increasing disorder one recovers its topological nature ($W_c \approx 210$ meV). Since there is no time reversal symmetry due to the finite exchange field, the spin-Chern insulator is re-instantiated as is the case for the panels (c), (d) and (e), (f) of Fig. 3 of the main text. Further increasing the disorder drives the system to an Anderson insulator. The QAH to spin-Chern insulator transition is described well by the self-consistent Born approximation.

V. INFLUENCE OF THE CHOICE OF LEADS

Here, we explicitly discuss the influence of choosing different leads on the calculated transport properties shown in the main text, where the lead was chosen in the QSH phase. The main reason why we use the QSH lead is to probe the disorder-induced TPT in the central region most clearly. Using a lead with a trivial bulk gap (such as the clean TI thin film with the thickness of 3QLs), the system is blind to probe the conductance inside the energy window of the band gap, which is the most interesting region to observe the new physics. This is trivial as, since without doping, the Fermi energy $E_F = 0$ is firmly inside of the leads bulk gap and therefore we would not be able to detect the new disorder induced topological phases in the central region. Alternatively, we need to dope the lead to be metallic. Therefore, we also compare the transport properties calculated for QSH lead with those for such a metallic lead. The latter might be connected closer to the current experimental setup routinely realized. In the metallic case, we can probe the transport signal inside the band gap of the TI thin films and the same physics as shown in the case of the QSH lead can be found. However, due to residual hybridization between the lead and central region, the physics shows up even more clearly with the QSH lead, which we preferred to choose.

In the following part, we compare the transport properties probed by using these three different kinds of leads: (1) lead of the same nature as the central region but in the clean limit, (2) metallic lead, and (3) QSH lead. Type (1) is defined as using the disorder-free magnetically doped TI thin films which is the same material

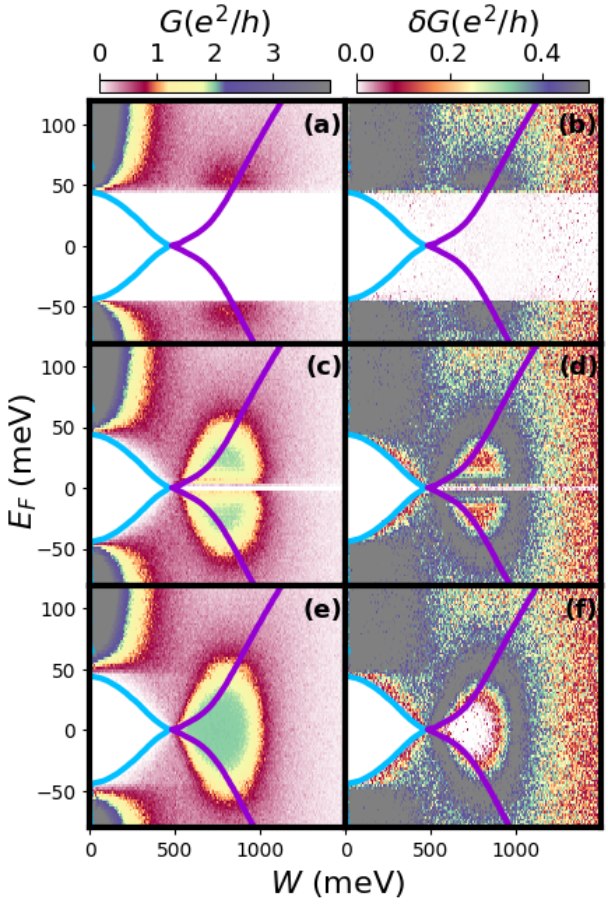

FIG. 2. Left (a), (c), (e) and right (b), (d), (f) panels show the average conductance G and the corresponding standard deviation δG as a function of disorder strength W and Fermi Energy E_F for 3QLs TI thin film without magnetic doping. Lead types are (a), (b) lead of same type as in the central region, but in the clean limit, (c), (d) metallic lead and (e), (f) QSH lead.The exchange fields gM are taken to be 0 meV. The other parameters and the meaning of the solid and dashed lines are shown in Ref. 2. In all calculations, the system sizes are set to $L_x = 400a$ and $L_y = 100a$ and averages over 50 random configuration are performed.

used for the central region (without disorder, namely $W = 0$). The mass of the left and right lead region $m^{u/l}_{0,L/R}$ is set equal to the the central one $m^{u/l}_{0,C}$. Such setups have been used in many previous works.[3,4] In the cases of type (2) and (3), we do not consider any disorder and magnetic doping in the leads. We define the type (2) lead by setting $m^{u/l}_{0,L/R} = 0$, where the lead is a semi-metal. For a type (3) lead, we keep all parameters in the intrinsic TI thin film unchanged except the mass term. In order for the lead to be a QSH insulator with the same bulk gap as the original material used in the central region (without disorder, namely $W = 0$), we always define the sign of the mass term to be negative, namely $m_{0,L/R}$=$-|m^u_{0,C}|$ for $|m^u_{0,C}| < |m^l_{0,C}|$ and

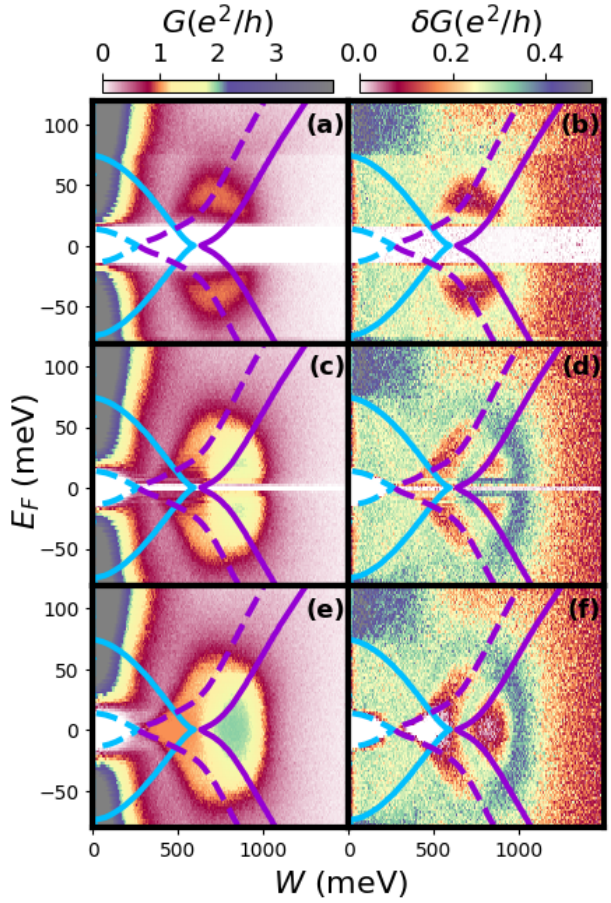

FIG. 3. Left (a), (c), (e) and right (b), (d), (f) panels show the average conductance G and the corresponding standard deviation δG as a function of disorder strength W and Fermi Energy E_F for 3QLs TI thin films with doping. Lead types are (a), (b) lead of same type as in the central region, but in the clean limit, (c), (d) metallic lead and (e), (f) QSH lead. The exchange fields gM are taken to be 30 meV. The other parameters and the meaning of the solid and dashed lines are shown in Ref. 2. In all calculations, the system sizes are set to $L_x = 400a$ and $L_y = 100a$ and averages over 50 random configuration are performed.

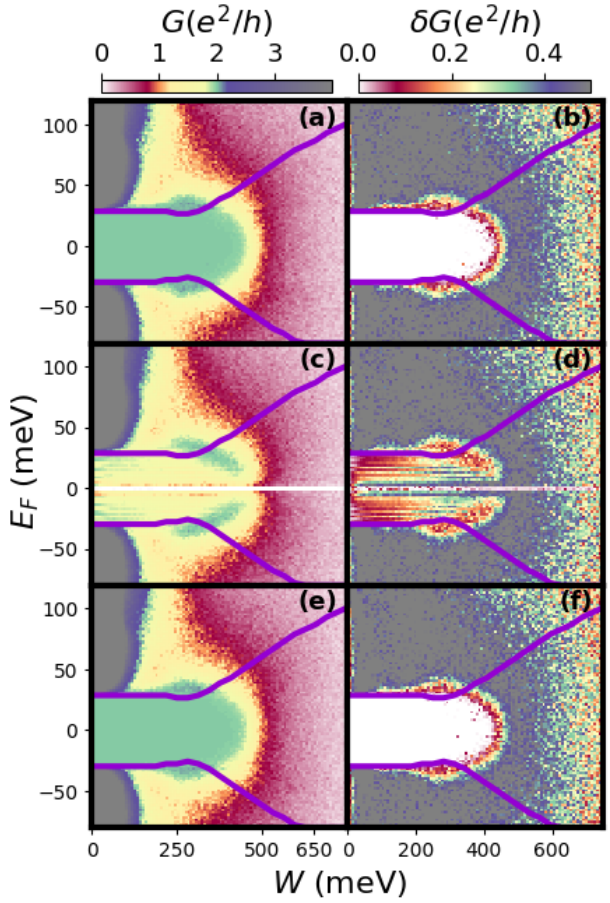

FIG. 4. Left (a), (c), (e) and right (b), (d), (f) panels show the average conductance G and the corresponding standard deviation δG as a function of disorder strength W and Fermi Energy E_F for 4QL TI thin film without magnetic doping. Lead types are (a), (b) normal sample lead (c), (d) metallic lead (e), (f) QSH lead. The exchange fields gM are taken to be 0 meV. The other parameters and the meaning of the solid and dashed lines are shown in Ref. 2. In all calculations, the system sizes are set to $L_x = 400a$ and $L_y = 100a$ and averages over 50 random configuration are performed.

$m_{0,L/R}$=$-|m^l_{0,C}|$ for $|m^l_{0,C}| < |m^u_{0,C}|$. The bulk gap value of the QSH leads in the above two cases depends on the magnitudes of $|m^u_{0,C}|$ and $|m^l_{0,C}|$. So in this case within the lead, the helical edge channel always exist ($G = 2e^2/h$), which can connect to edge states and bulk metallic states in the central regions.

In Figs. 2 and 3, we show the phase diagram of 3QLs with a choice of several different leads. Figures 2 (a), (b) and 3 (a), (b) clearly show that the conductance vanishes in the energy window of bulk gap and we cannot observe TPTs with the choice of type (1) as a lead. This is because there is no charge transport from the left lead to the right within the gap energy window even if the central region is metallic. This effect has already been mentioned briefly in Ref. 1, where highly doped leads were used to avoid suffering from this blind spot (compare to Fig. 1 in Ref. 1 and Fig. 2(f) in Ref. 3).

Although with the choice of metallic lead, we can observe the disorder induced TPTs inside the band gap of TI thin films shown in Figs. 2 (c), (d) and 3 (c), (d), their edge state conductance obtained with metallic leads is not as clear as QSH leads. In Figs. 2 (e), (f) and 3 (e), (f), where a QSH lead is employed, clear signatures of edge state transport ($G = 2e^2/h$ or e^2/h, and vanishing standard deviation δG as discussed in the main text) can be observed. The reason may lie in interface effect between the semi-metallic lead and the central region. The work about this interface effect and choice of leads will be systematically studied in a future paper. Even though in Fig. 3 (f), the standard deviation corresponding to the spin-Chern insulator is not exactly vanishing, this is a

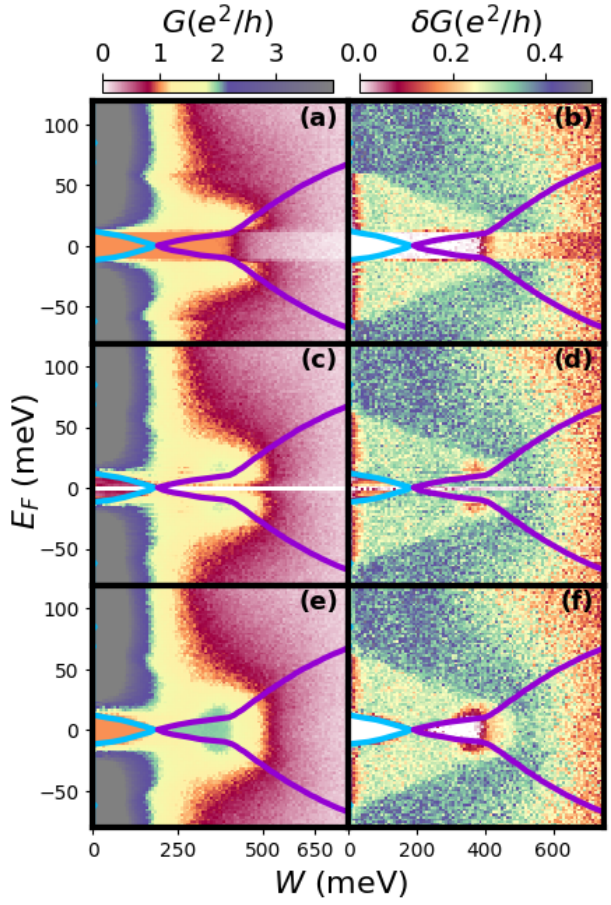

FIG. 5. Left (a), (c), (e) and right (b), (d), (f) panels show the average conductance G and the corresponding standard deviation δG as a function of disorder strength W and Fermi Energy E_F for 4QLs TI thin film with magnetic doping. Lead types are (a), (b) lead of same type as in the central region, but in the clean limit, (c), (d) metallic lead and (e), (f) QSH lead. The exchange fields gM are taken to be 40 meV. The other parameters and the meaning of the solid and dashed lines are shown in Ref. 2. In all calculations, the system sizes are set to $L_x = 400a$ and $L_y = 100a$ and averages over 50 random configuration are performed.

finite size effect. This can be clearly seen by comparing Fig. 3 (f) with Fig. 3 (d) in the main text, where the former uses $Ny = 100$ whereas the latter uses $Ny = 200$.

In Fig. 4, we show the transport properties of 4QLs thin films comparing the influence of choosing different leads. Because, by definition, case (1) is also a QSH lead, cases (1) and (3) as choices of leads are equivalent and consequently the same results are observed in Figs. 4 (a), (b) and (e), (f). In the case of a metallic lead, shown in Figs. 4 (c), (d), the QSH phase clearly detected inside the bulk gap for QSH leads (see Figs. 4 (a), (b) and (e), (f)), cannot be clearly obtained due to the interface effect using metallic leads.

In the case of finite exchange field as shown in Fig. 5, corresponding to QAH phase without disorder, we can see the same phenomena discussed in Figs. 2 and 3. With the choice (1) for a lead, we cannot clearly detect the TPTs from the QAH to the spin-Chern insulator because the largest current of the lead ($G = e^2/h$) is smaller than the edge conductance of spin-Chern insulator ($G = 2e^2/h$). However, since the QSH lead hosts the edge current of $G = 2e^2/h$, we can observe the TPT induced by disorder from a QAH to spin-Chern insulator in the central region when using a QSH lead. Although, for metallic leads similar trait can be seen in Figs. 5 (c), (d) as in (e), (f), the signature of edge state conductance is not as clear as in the case of QSH leads again due to interface effect.

* peizhet@buaa.edu.cn
† Dante.Kennes@rwth-aachen.de

[1] C. W. Groth, M. Wimmer, A. R. Akhmerov, J. Tworzydło, and C. W. J. Beenakker, Phys. Rev. Lett. **103**, 196805 (2009).

[2] The parameters in simulations are $v_F = 3.07/2.36$ eV Å, $m_0 = 44/-29$ meV, $B = 37.3/12.9$ eV Å^2 for $(Bi, Sb)_2Te_3$ thin film with thickness of 3QLs/4QLs[5]. Solid and dash lines correspond to phase boundaries calculated from the self-consistent Born approximation for the upper and lower block of the Hamiltonian. The blue and purple lines show $|\overline{\mu}^{u/l}| = \overline{m}_0^{u/l}$ and $|\overline{\mu}^{u/l}| = -\overline{m}_0^{u/l}$, respectively.

[3] J. Li, R.-L. Chu, J. K. Jain, and S.-Q. Shen, Phys. Rev. Lett. **102**, 136806 (2009).
[4] H. Jiang, L. Wang, Q.-f. Sun, and X. C. Xie, Phys. Rev. B **80**, 165316 (2009).
[5] J. Wang, B. Lian, and S.-C. Zhang, Phys. Rev. Lett. **115**, 036805 (2015).